Rule-Based Models with Generative Adversarial Networks: A Deepwater Lobe, Deep Learning Example

Conference Paper · September 2019

DOI: 10.1306/42402Jo2019

3 authors, including:

Honggeun Jo
University of Texas at Austin
17 PUBLICATIONS **138** CITATIONS

SEE PROFILE

Javier E. Santos
University of Texas at Austin
19 PUBLICATIONS **94** CITATIONS

SEE PROFILE

Click to view slide presentation

[EA]Conditioning Stratigraphic, Rule-Based Models with Generative Adversarial Networks: A Deepwater Lobe, Deep Learning Example*

Honggeun Jo[1], Javier E. Santos[1], and Michael J. Pyrcz[1,2]

Search and Discovery Article #42402 (2019)**
Posted August 5, 2019

*Adapted from extended abstract prepared in conjunction with oral presentation given at 2019 AAPG Annual Convention and Exhibition, San Antonio, Texas, May 19-22, 2019
 DOI:10.1306/42402Jo2019

[1]The University of Texas at Austin, Austin, TX (honggeun.jo@utexas.edu)
[2]Bureau of Economic Geology, The University of Texas at Austin, TX

Abstract

A stratigraphic, rule-based reservoir modeling method simulates sedimentary dynamics to generate numerical descriptions of reservoir architecture while capturing geological processes informed features. However, robust conditioning of these models to local data (i.e., well log interpretation, core data, and seismic constraints) remains a significant obstacle to a broad application for subsurface modeling. A novel deep learning-based method is proposed for the fast and flexible conditioning in this study.

This study includes a recently designed rule-based modeling method for a deepwater lobe reservoir, controlled by three geological parameters: 1) the compositional exponent, 2) the lobe geometry, and 3) the distribution of petrophysical properties within the lobes. The compositional exponent tunes the placement rule of lobe elements based on the elevation of the previous composite surface. The geometries of the lobe elements are characterized by parameters representing their radius and thickness. After building the reservoir structure, the rule-based method allocates petrophysical properties (i.e., porosity and permeability) bounded by surfaces with a hierarchical trend model, parameterized by gradients, orientations, mean, and standard deviation. Our deep learning-based, local data conditioning workflow consists of four steps: 1) training Generative Adversarial Networks (GANs) with the rule-based models, 2) making voids in a rule-based model near well locations, 3) assigning local data at the well locations, and 4) filling the rest voids with the most optimum GANs realization via semantic image inpainting. GANs use the multiple training data (i.e., the rule-based models) to extract the primary geological features and generate reservoir models that preserve these features. With the trained GANs, it is possible to explore the latent reservoir model manifold and identify the optimum models that satisfy the given local data. Semantic image inpainting scheme enables the trained GANs to find the optimum voids that are harmonic with the surrounding regions and generate a realistic realization. This workflow results in subsurface models that honor the complicated geological-based heterogeneities while being consistent with the well data.

An experiment based on a deepwater depositional complex demonstrates that our approach successfully captures the geological rules through the primary geological features. Moreover, the approach honors local data while rendering realistic reservoir heterogeneity, continuity, and spatial distribution of petrophysical parameters. The flexibility of the rule-based modeling method combined with GANs allows this approach to be applied to various depositional systems.

Introduction

Rule-based models are generated by applying depositional process, informed rules in temporal sequence to modify topographic surfaces and preserve sediment units. Rule-based modeling is referred to as event-based (Pyrcz et al., 2006), hybrid (Michael et al., 2010), surface-based (Pyrcz et al., 2005; Bertoncello et al., 2013), process-oriented (Wen, 2005) and rule-based modeling (Pyrcz et al., 2015; Jo et al., 2019). These methods enable us to build reservoir models to integrate geologic concepts and preserve geologic heterogeneity and continuity which are not readily achievable with other conventional geostatistical method (e.g., variogram-based, object-based, and multipoint-based).

While rule-based models are emerging in applications for both of deepwater and fluvial clastic reservoirs, there is a remaining obstacle to a broad application: conditioning to well data due to rule-based models' stochastic aspect (Pyrcz et al., 2015). Pyrcz (2004) iterate to generate most optimum stratigraphic surface and add stochastic residuals to match well data. Michael et al. (2010) suggest combination of rule-based modeling method and conventional geostatistical methods to solve this problem. Bertoncello et al. (2013) pick the most sensitive parameters of rule-based model by sensitivity analysis and apply sequential optimization scheme to find the optimum values. However, these methods are only applicable in sparse well data cases. When well data are dense none of these methods perform well.

Generative Adversarial Networks (GANs) is a framework for estimating generative models through an adversarial process, where two models are trained concurrently: a generative model and a discriminative model (Goodfellow et al., 2014). GANs pose an advantage in generating new realizations which are not exactly same as training data (i.e., a realization is not simply sampled from the known data) and representing high-resolution images, comparing with other methods based on Markov chains. Radford et al. (2015) suggest Deep Convolutional GAN (DCGAN) where convolutional networks (CNNs) is adopted to capture geometric configuration of images better. Wu et al. (2016) expand application of GANs to 3D objects and verify that it is possible to capture 3D configuration of objects with a 3D kernel. Yeh et al. (2016) suggest sematic image inpainting algorithm with DCGAN which generates the missing content of 2D image by conditioning on the available data. Given a trained DCGAN, missing content is estimated through navigating the latent image manifold and minimizing semantic loss, which consists of perceptual and conceptual loss (Yeh et al., 2016).

Our novel contribution in this work is applying DCGAN and semantic image inpainting to local data conditioning problem of rule-based models. With multiple rule-based models, DCGAN is trained in purpose of extracting the main geological features and generating the latent reservoir manifold. After training GANs, void areas are generated near well locations in a rule-based model. Well data are assigned at the well locations and the rest voids are filled with a DCGAN realization by navigating the latent reservoir manifold. Semantic image inpainting scheme helps DCGAN to find the most optimum reservoir model that makes the voids compatible with the surrounding area and looks geologically realistic.

Method

Rule-based modeling method

In this study, rule-based models are designed for deepwater lobe depositional system. One rule-based model consists of multiple lobe elements (around 10 ~ 30) to build lobe or lobe complex. The lobe geometry is affected by 1) turbidity flow properties, 2) the frequency of flows, 3) gradient change and seafloor morphology and so on (Deptuck et al., 2008). A simplified ellipsoidal lobe geometry is assumed as shown in Figure 1. The model starts with an initial bathymetry and then sequentially adds lobe elements to fill the model. Each lobe element deposit modifies the surface in an aggradational manner. Figure 2 shows the workflow of the rule-based model which uses an identical concept of Xie et al. (2001), Pyrcz et al. (2005), and Jo et al. (2019).

Our rule-based model is mainly controlled by three geological parameters: 1) the compositional exponent, 2) the lobe geometry, and 3) the distribution of petrophysical properties within the lobes. The compositional exponent ranges from 0 (i.e., random stacking) to 5 (i.e., perfect compensational stacking) and determines the stacking pattern of lobe reservoir. Since an ellipsoidal lobe geometry is assumed, radius and thickness should be described to define lobe geometry. After building the reservoir structure, the rule-based method distributes petrophysical properties (i.e., porosity and permeability) with a hierarchical trend model, ranging from 0 to 1 and representing the quality of reservoir (i.e., 0 indicates fine-grained, poor quality whereas 1 indicates coarse-grained, good quality). The reservoir extent is 5.6 km × 5.6 km × 40 m, consisting of 28 × 28 × 20 grid cells. Therefore, individual grid cell has 200 m × 200 m × 2 m dimension in x, y, and z direction, respectively. Moreover, perfect compensational stacking pattern, 1.7 km of lobe element radius, and 8 m of lobe element thickness are assumed in this work.

Figure 3 shows an example of the rule-based model. Quality of the reservoir is determined by the hierarchical trend model after building compositional surface and ranges between 0 and 1. For individual lobe element, high permeability and porosity sand facies are located in the center and poor-quality shale drapes exist on the surface. Overall, coarsening-up trend is overserved in the reservoir.

Deep Convolutional Generative Adversarial Networks

GANs are a framework for training generative models in an adversarial manner against discriminative models and have been verified to generate high-resolution images (Goodfellow et al., 2014; Denton et al., 2015). To capture local connectivity patterns of images, CNNs have been applied to GANs and this scheme is named DCGAN (Radford et al., 2015). Generative model, G, maps a random vector $\mathbf{z}$, sampled from a prior distribution to the image space while Discriminative model, D, maps an input image to a likelihood of true image (0 for fake and 1 for true). The G and D are trained by optimizing the following loss function:

$$\min_G \max_D V(G,D) = \mathbb{E}_{\boldsymbol{h}}\left[\log(D(\boldsymbol{h}))\right] + \mathbb{E}_{\boldsymbol{z}}\left[\log(1 - D\big(G(\boldsymbol{z})\big)\right], \quad (1)$$

where $\boldsymbol{h}$ is the sample from real images and $\boldsymbol{z}$ is random variables from the latent space.

For training DCGAN for rule-based models, a 3D image, this requires utilization of a 3D kernel in CNNs. Figure 4 represents the schematic diagram of DCGAN. Discriminative model gets input 3D image from either rule-based models (true) or realization of generative models (fake) and assigns a probability that the input is sampled from rule-based models. The latent random variables are 100, individually sampled from a Gaussian distribution with a mean of zero and unity variance. 40,000 rule-based models were used to train the DCGAN over 30,000 iterations with 40 batch size, which required about 8 hours on a desktop with an Nvidia M6000 GPU.

The CNNs structure of generative model is shown in Figure 5. The approach includes activation functions, batch normalization, and pooling/striding methods, following Radford et al. (2015). After analyzing sensitivity of other hyperparameters, the modeled is tuned to the following CNNs (Figure 5) structure that performed optimally for this study. However, if the extent of reservoir is changed, the feature map size of feature map and the number of channels must be updated accordingly.

Well data conditioning via Semantic Image Inpainting

Two types of information should be considered in the inpainting task: contextual and perceptual information. For a corrupted image with some missing regions, the missed pixels (or voxels in 3D image) should be inferred based on the surrounding pixels (or voxels). Moreover, the filled parts should be "realistic" in that they have features similar to the training data. The former information is contextual information and the latter one is perceptual information. Semantic inpainting integrates both conceptual loss and perceptual loss (Yeh et al., 2016), to determine the missing parts of an image through minimizing the following semantic loss function:

$$L_{semantic}(\mathbf{z}) \equiv L_{conceptual}(\mathbf{z}) + \lambda \cdot L_{perceptual}(\mathbf{z}), \tag{2}$$

$$L_{conceptual}(\mathbf{z}) = \|\mathbf{M} \odot G(\boldsymbol{z}) - \mathbf{M} \odot y\|_1, \tag{3}$$

$$L_{perceptual}(\mathbf{z}) = \log(1 - D(G(\mathbf{z}))), \tag{4}$$

where **M** is the mask (matrix with elements 0 for missing portions and 1 for the rest), $\odot$ is element-wise multiplication, λ is a hyperparameter to control significance of conceptual and perceptual information for the inpainting, and **y** is the corrupted image.

With trained DCGAN and semantic image inpainting scheme, this study proposes a novel method to solve well data conditioning problem of the rule-based model. After generating a rule-based model, our proposed method places voids in the adjacent areas of well locations, hard data (from either well logs or core samples) are assigned to the center of voids. Semantic loss is defined and $\mathbf{z}$ is optimized by gradient descent. The masked rule-based model and $G(\boldsymbol{z}_{\boldsymbol{optimum}})$ are blended to reconstruct whole reservoir model. Overall workflow is described in Figure 6.

Results

DCGAN for rule-based models

Trained DCGAN gives realistic models as shown in Figure 7. Figure 7(a) is the 3D view of the rule-based model and Figure 7(b) shows a realization of DCGAN with random variable $\boldsymbol{z}$. Distinct shale drapes of lobe elements are observed in both of rule-based model and a DCGAN realization. Moreover, cross-sectional areas of the DCGAN result show the same lobe geometry and stacking rule are found in both horizontal and vertical layers as visualized in Figure 7(c). Since ellipsoidal, uniform lobe elements and perfect compensational stacking pattern are defined in training data, DCGAN realization also shows ellipsoidal, uniform lobe elements, and perfect compensational pattern.

As DCGAN takes continuous random variables to generate 3D images, continuous change of 3D images are expected by changing random variables in a gradual manner and inputting them to DCGAN. Figure 8 shows the gradual change of 3D images between realizations of $G(\mathbf{z_1})$ and $G(\mathbf{z_2})$. The fact, that $G(\mathbf{z})$ is changed continuously by the continuous change of random variables **z,** enable us to explore the latent reservoir manifold and apply gradient descent scheme to DCGAN for the optimization problem.

Well data conditioning

After generating a rule-based model, voids are assigned near wells and well data in the center of voids are input. Mask is a 3D matrix which consists of either 0 (for void) or 1 (for the rest). The element-wise multiplication of the rule-based model and the mask enable us to make the voids. The radius of a void area is defined as around 1 km and this should be adjusted depending on the density of well data. Figure 9 represents the process to make voids in a rule-based model.

The voids should be filled by DCGAN, $G(\mathbf{z})$, and the related random variables, $\mathbf{z}$, is determined by minimizing $L_{semantic}$ of equation (2). Due to the continuous characteristic of $G(\mathbf{z})$, gradient descent is applicable to this optimization. After finding $\mathbf{z_{optimum}}$, the voided model can be combined with $G(\mathbf{z_{optimum}})$ to reconstruct the complete model. Figure 10(a) shows a 3D view of the reconstructed model and Figure 10(b) and Figure 10(c) represent the cross-sectional view of the voided and reconstructed model. The proposed method assures spatial continuity of the reservoir model to be preserved in both horizontal and vertical layers. Especially, shale drapes of lobe elements are well connected and stacking pattern does not significantly change. On top of quantitative analysis, when the reconstructed model is input into discriminative model, $D(G(\mathbf{z_{optimum}})$, the probability of $G(\mathbf{z}_{\text{optimization}})$ is sampled from the training data (i.e., rule-based model set) is turned out to be over 99%. Therefore, these results verify that DCGAN and semantic image inpainting can solve well data conditioning of the rule-based model.

Discussion

With a trained DCGAN, this study demonstrates that DCGAN can realize 3D lobe reservoirs which conserve geological features that are controlled by geological parameters in rule-based modeling method. Since DCGAN realization follows a different distribution, CDF mapping is required to conserve the original bimodal distribution of reservoir properties. Continuous characteristic of DCGAN realization enables us to

use gradient descent optimization. Though semantic image inpainting algorithm, the proposed method successfully solves well conditioning problem, not only for horizontal continuity but also for vertical continuity.

Conclusion and Future Work

In this paper, a novel deep learning-based method is proposed for well data conditioning in rule-based models. Compared to existing methods based on conventional geostatistics, the proposed method has more flexibility in preserving hard data in reservoir models and larger computational efficiency once a trained DCGAN is given. Even though future works are required to tackle some issues of instability in training DCGAN – generative model shows oscillating loss function after certain amount of iterations, this study demonstrates our generative model can render sharp and realistic 3D reservoir models. Extending this framework to other application such as history matching (i.e., navigating the latent reservoir manifold to find the optimum reservoir models) and integration of geologic information (i.e., adding stratigraphic surface from seismic interpretation via conditional GAN) should be very interesting.

Selected References

Bertoncello, A., T. Sun, H. Li, G. Mariethoz, and J. Caers, 2013, Conditioning Surface-Based Geological Models to Well and Thickness Data: Mathematical Geosciences, v. 45/7, p. 873-893.

Denton, E.L., S. Chintala, and R. Fergus, 2015, Deep Generative Image Models Using a Laplacian Pyramid of Adversarial Networks: Advances in Neural Information Processing Systems, p. 1486-1494.

Deptuck, M.E., D.J.W. Piper, B. Savoye, and A. Gervas, 2008, Dimensions and Architecture of Late Pleistocene Submarine Lobes Off the Northern Margin of East Corsica: Sedimentology, v. 55, p. 869-898.

Goodfellow, I., J. Pouget-Abadie, M. Mirza, B. Xu, D. Warde-Farley, S. Ozair, A. Courville, and Y. Bengio, 2014, Generative Adversarial Nets: Advances in Neural Information Processing Systems, p. 2672-2680.

Jo, H., and M.J. Pyrcz, 2019, Robust Rule-Based Aggradiational Lobe Reservoir Models: In Proceedings of the Natural Resources Research.

Michael, H.A., H. Li, A. Boucher, T. Sun, J. Caers, and S.M. Gorelick, 2010, Combining Geologic-Process Models and Geostatistics for Conditional Simulation of 3-D Subsurface Heterogeneity: Water Resources Research, v. 46/5, 20 p. doi:10.1029/2009WR008414

Mutti, E., and W.R. Normark, 1987, Comparing Examples of Modern and Ancient Turbidite Systems: Problems and Concepts, *in* J.K. Leggert and G.G. Zuffa (eds.), Marine Clastic Sedimentology; Concepts and Case Studies: Graham and Trotman, London, p. 1-38.

Pyrcz, M.J., 2004, Integration of Geologic Information into Geostatistical Models: Ph.D. Thesis, University of Alberta, Edmonton, Alberta, 296 p.

Pyrcz, M.J., O. Catuneanu, and C.V. Deutsch, 2005, Stochastic Surface-Based Modeling of Turbidite Lobes: American Association of Petroeleum Geologists Bulletin, v. 89/2, p. 177-191.

Pyrcz, M.J., S. Strebelle, R.M. Slatt, N.C. Rosen, M. Bowman, J. Castagna, and R. Smith, 2006, Event-Based Geostatistical Modeling of Deepwater Systems: In Gulf Coast Section SEPM 26th Bob F. Perkins Research Conference, p. 893-922.

Pyrcz, M.J., R.P. Sech, J.A. Covault, B.J. Willis, Z. Sylvester, and T. Sun, 2015, Stratigraphic Rule-Based Reservoir Modeling: Bulletin of Canadian Petroleum Geology, v. 63/4, p. 287-303.

Radford, A., L. Metz, and S. Chintala, 2015, Unsupervised Representation Learning with Deep Convolutional Generative Adversarial Networks: arXiv preprint arXiv:1511.06434, 16 p.

Stow, D.A.V., and M. Johansson, 2000, Deep-Water Massive Sands: Nature, Origin and Hydrocarbon Implications: Marine and Petroleum Geology, v. 17, p. 145-174.

Straub, K.M., C. Paola, D. Mohrig, M.A. Wolinsky, and T. George, 2009, Compensational Stacking of Channelized Sedimentary Deposits: Journal of Sedimentary Research, v. 79, p. 673-688.

Straub, K.M., and D.R. Pyles, 2012, Quantifying the Hierarchical Organization of Compensation in Submarine Fans Using Surface Statistics: Journal of Sedimentary Research, v. 82, p. 889-898 doi:10.2110/jsr.2012.73

Wen, R., 2005, SBED Studio: An Integrated Workflow Solution for Multi-Scale Geo Modelling: 67th EAGE Conference and Exhibition, Madrid, Spain, 13–16 June 2005.

Wu, J., C. Zhang, T. Xue, B. Freeman, and J. Tenenbaum, 2016, Learning a Probabilistic Latent Space of Object Shapes Via 3D Generative-Adversarial Modeling: Advances in Neural Information Processing Systems, p. 82-90.

Xie, Y., A.S. Cullick, and C.V. Deutsch, 2001, Surface-Geometry and Trend Modeling for Integration of Stratigraphic Data in Reservoir Models: SPE Western Regional Meeting, Bakersfield, California, 26-30 March 2001, SPE 68817, 5 p.

Yeh, R.A., C. Chen, T.Y. Lim, A.G. Schwing, M. Hasegawa-Johnson, and M.N. Do, 2016, Semantic Image Inpainting with Deep Generative Models. arXiv preprint arXiv:1607.07539.

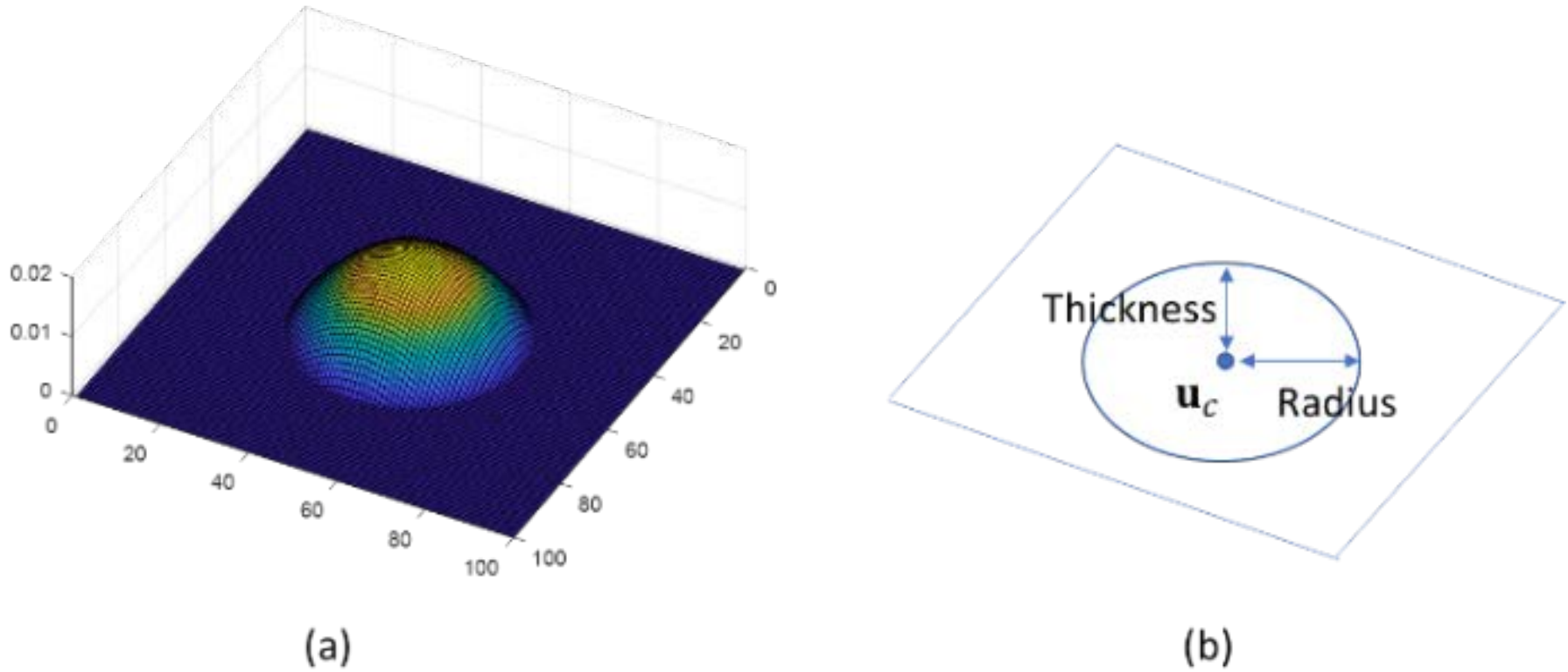

Figure 1. Lobe element geometry. (a) 3D view and (b) cross-sectional view.

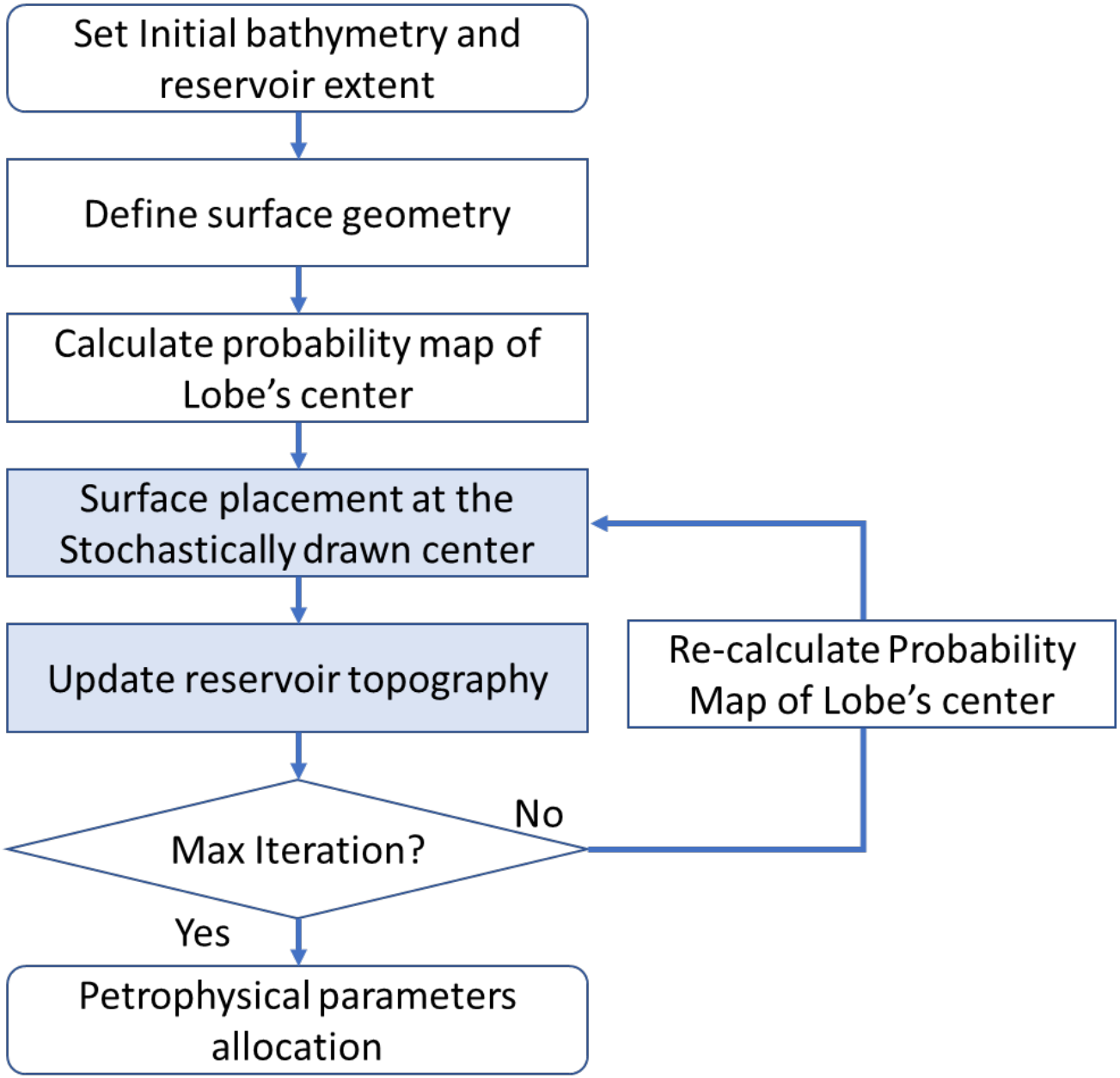

Figure 2. Flow chart of aggradational, rule-based model.

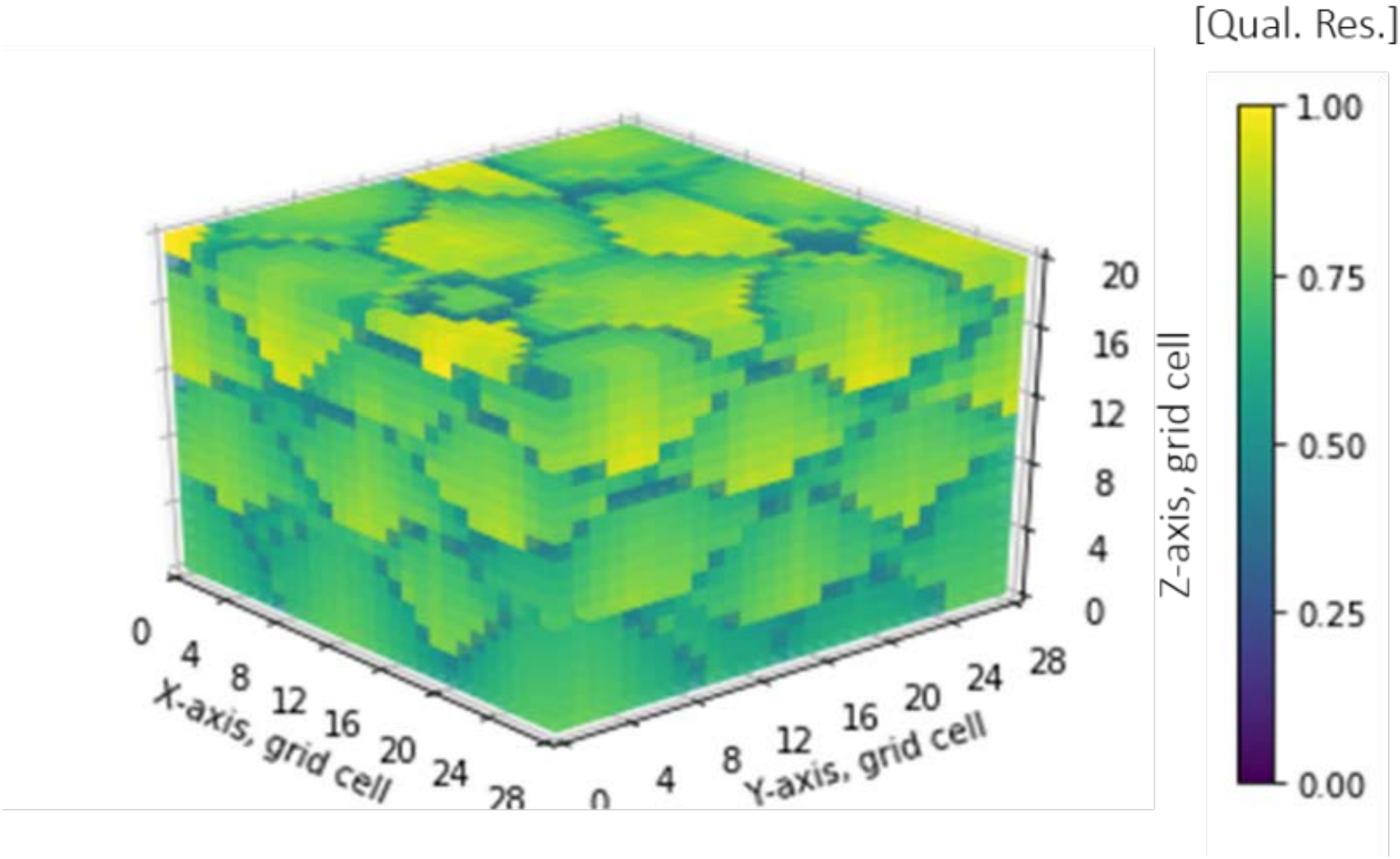

Figure 3. An example of rule-based model.

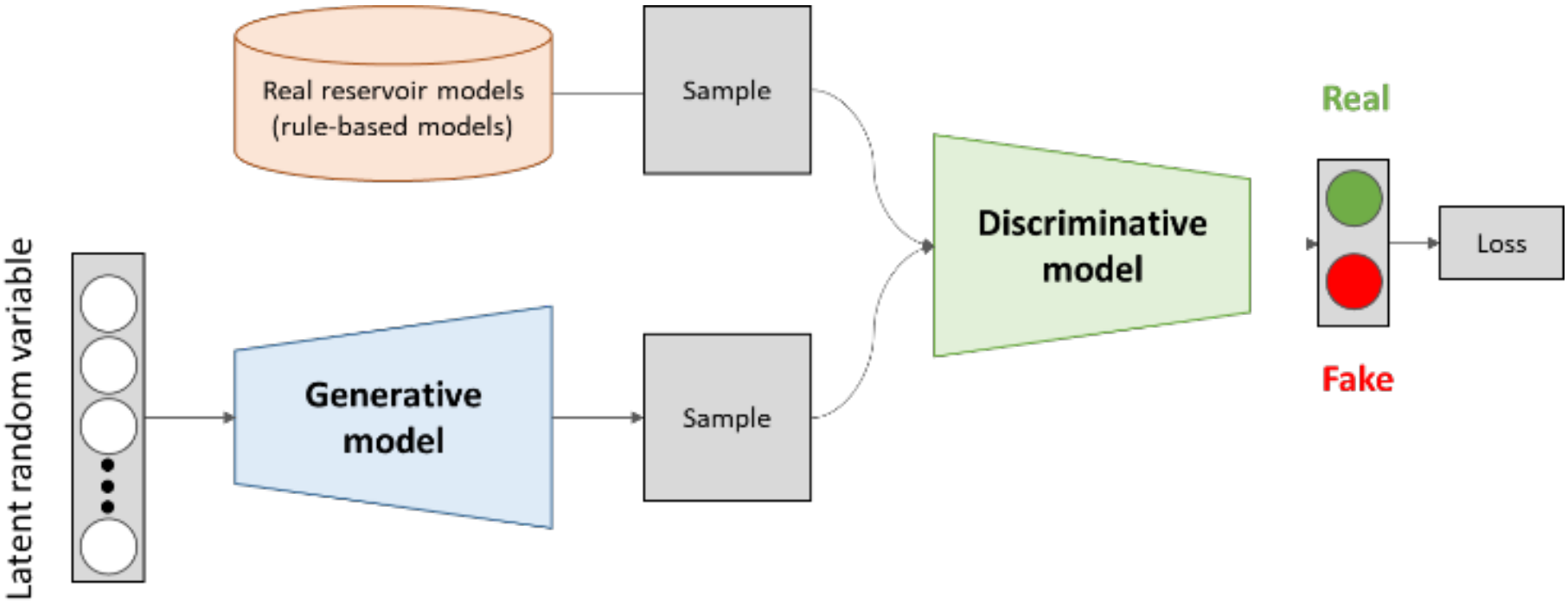

Figure 4. Schematic diagram of DCGAN.

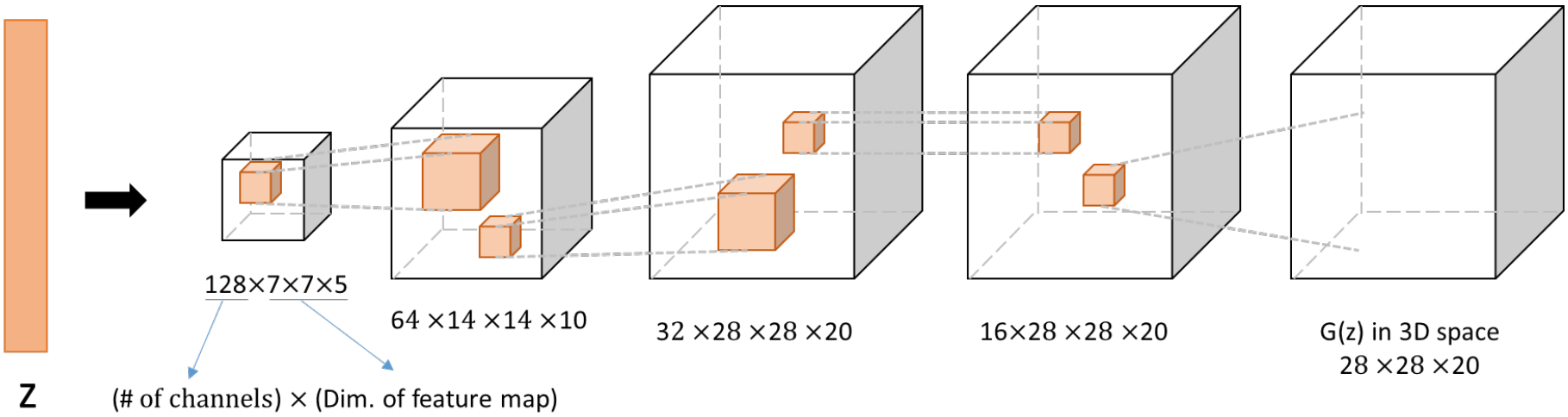

Figure 5. The structure of CNNs in DCGAN.

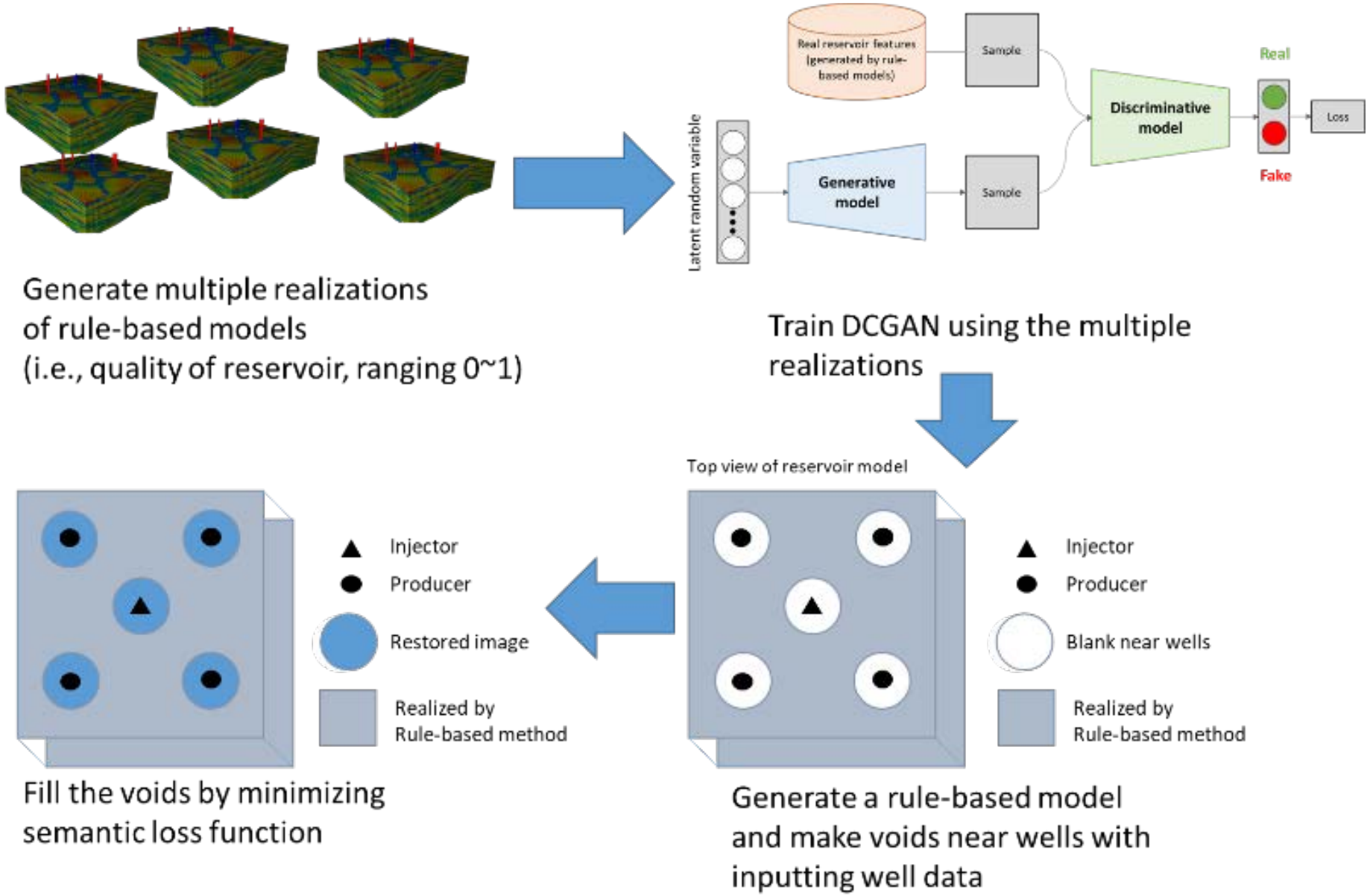

Figure 6. Workflow for well data conditioning.

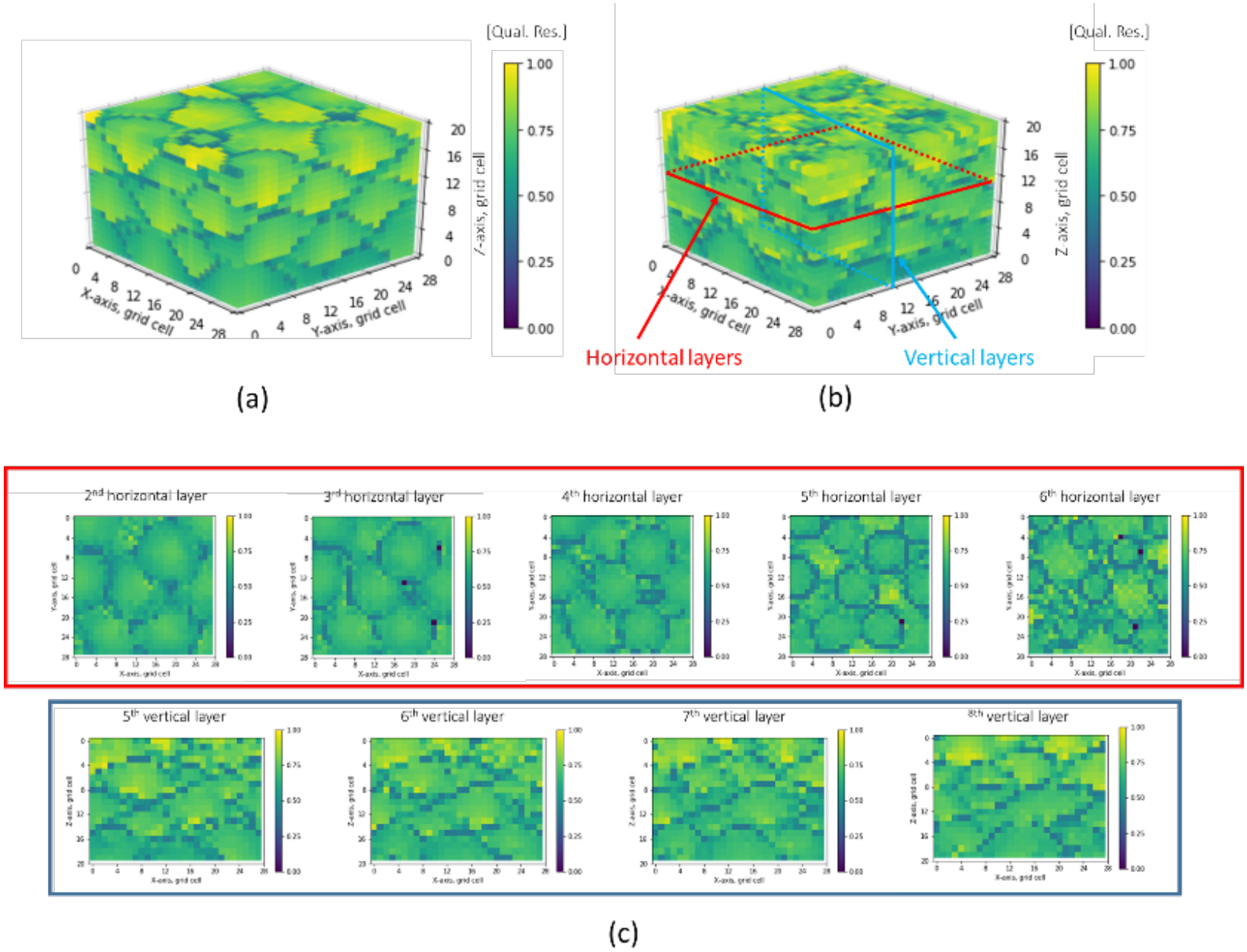

Figure 7. Comparison between rule-based model and DCGAN realization. (a) 3D view of rule-based model, (b) 3D view of DCGAN realization, and (c) cross-sectional view of DCGAN.

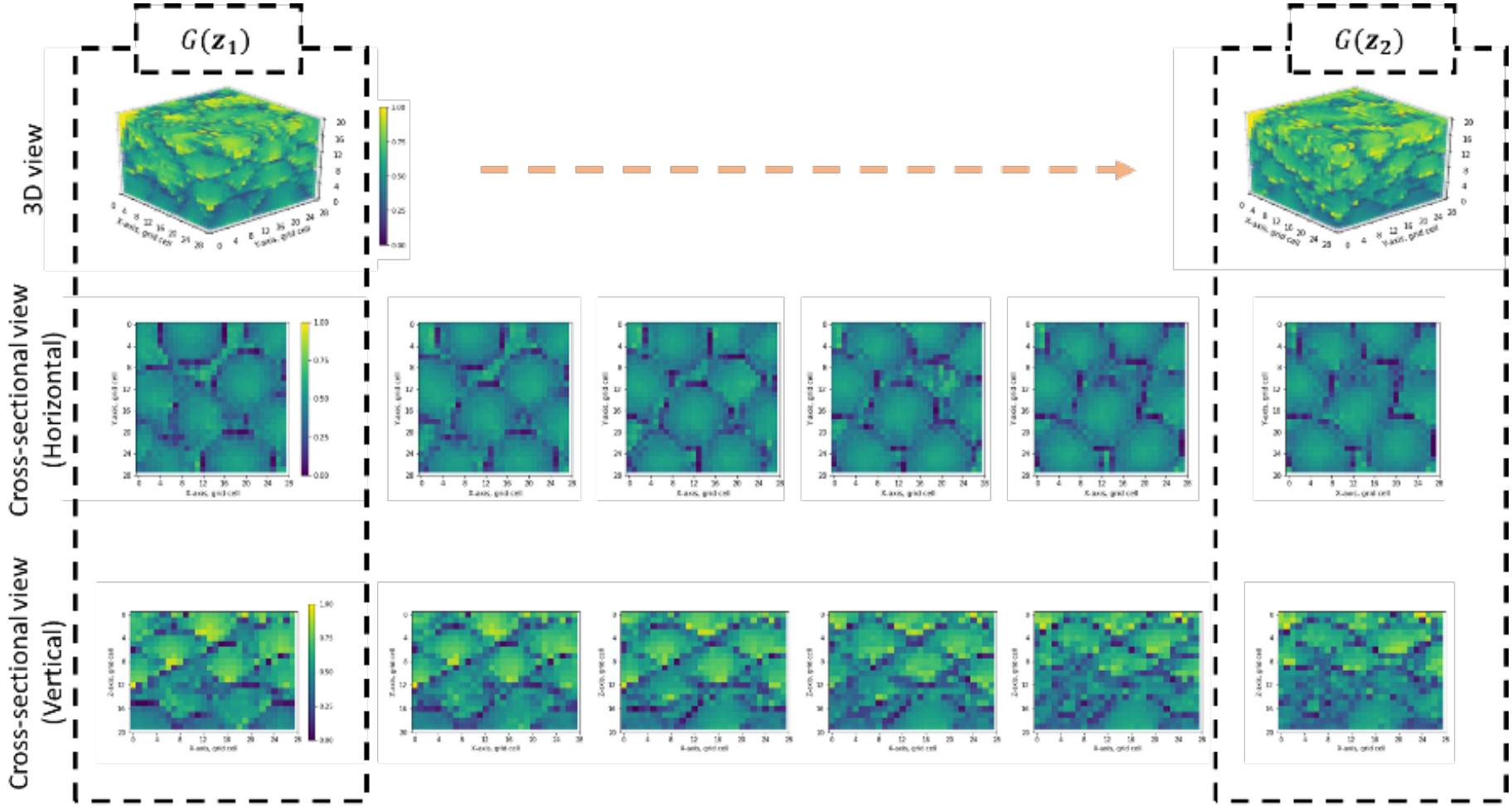

Figure 8. Continuous change of DCGAN realizations between two random variables $\boldsymbol{z_1}$ and $\boldsymbol{z_2}$.

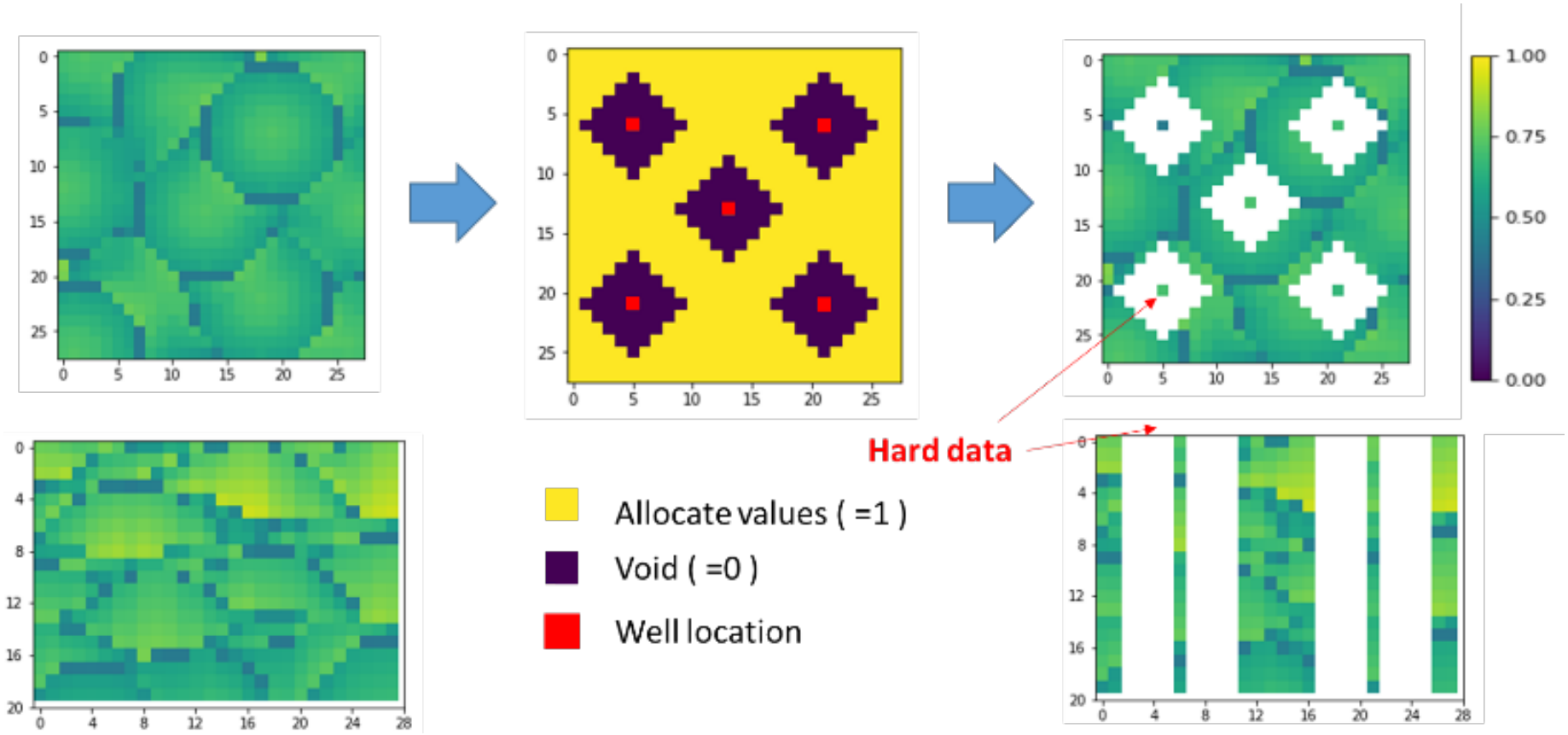

Figure 9. Rule-based model and mask.

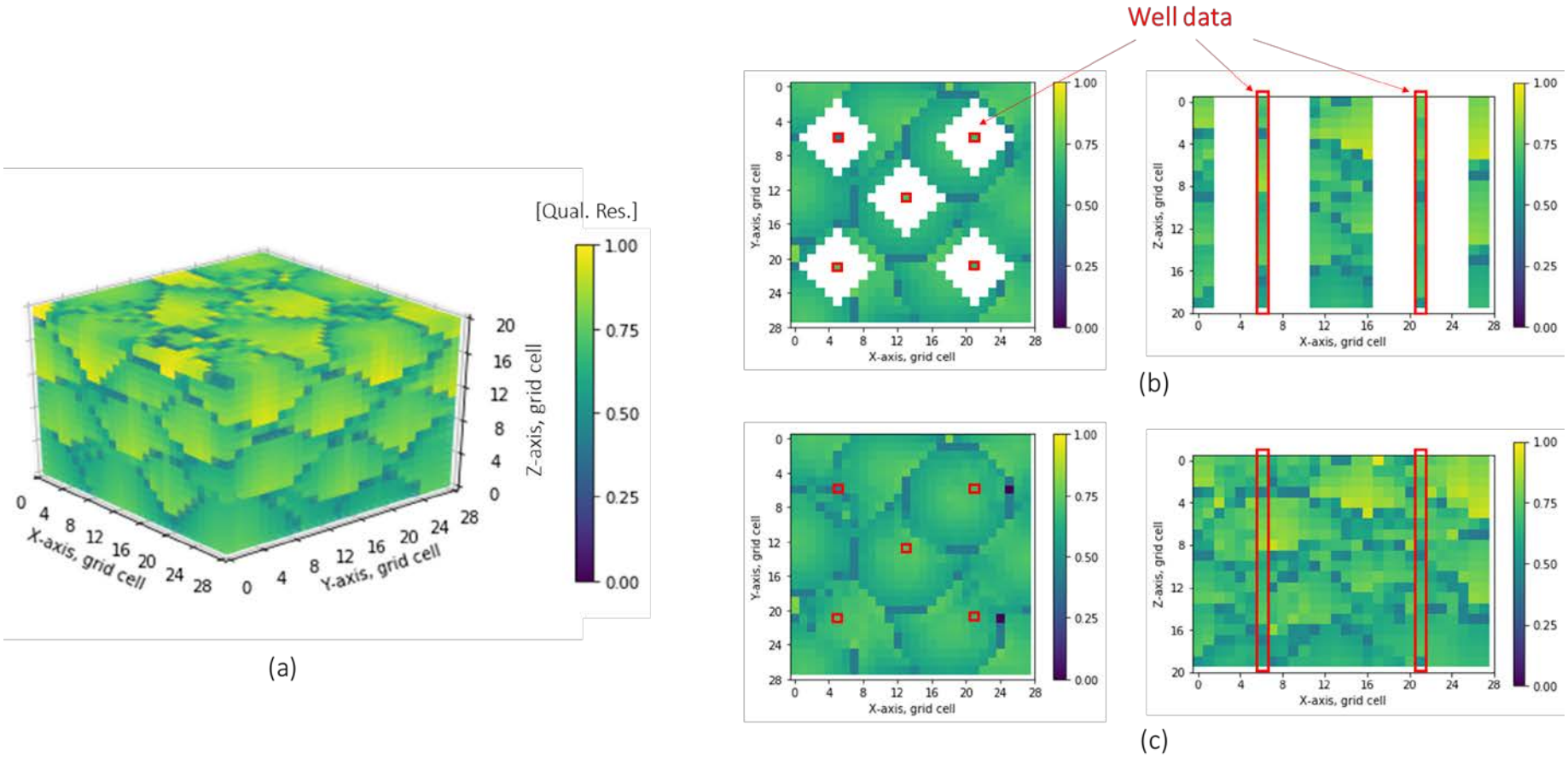

Figure 10. The reconstructed reservoir model and void area. (a) 3D view of the reconstructed model, (b) cross-sectional view of the voided model, and (c) cross-sectional view of the reconstructed model.